**The Compact Muon Solenoid Experiment**
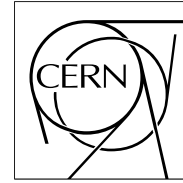
# CMS Note

Mailing address: CMS CERN, CH-1211 GENEVA 23, Switzerland

# Simulation of MSGC signals in CMS

Véronique Lefébure, for the Tracker Optimisation Group

*CERN, Geneva, Switzerland*

**Abstract**

The aim of this analysis is to compare the estimates of the CMS MSGC performance as reported in the Tracker TDR to the ones obtained with an ORCA simulation of the MSGC response including a detailed implementation of the signal deconvolution and a proper handling of event pile-up.

draft 5

# Contents

## 1   Introduction

The CMS MSGC performance estimates reported in the Tracker Technical Design Review (TDR [1]) were obtained without a complete simulation of the signal deconvolution logic. Its effect was approximated by applying signal reduction and noise increase factors but the contribution from off-time bunch crossing events could not be properly taken into account.

The analysis performed here uses ORCA [2], the Object-Oriented Reconstruction software for CMS Analysis, which enables pile-up of off-time bunch crossing interactions. In addition, the simulation of the MSGC response in ORCA includes a detailed implementation of the signal deconvolution.

The simulation of MSGC detector response is done in several steps as described in [3]. The detection of a particle starts with ionization of gas molecules along the trajectory. Primary electrons are occasionally produced with high kinetic energy (delta rays) and may further ionise the gas, creating secondary electrons. For simplicity we will call both kinds of electrons "primary electrons" to distinguish them from electrons created in the avalanche. Primary electrons drift and diffuse towards the multiplication region and produce the avalanche. Electrons are collected and so are ions, inducing the electric signal on the anodes and cathodes. Hits are reconstructed on the basis of the anode strip signals. Issues relevant to the subject of this analysis are explained in details in the following sections.

## 2   Raw Signal Shape

During the avalanche development, both the electrons drifting toward the anode strip and the ions moving away from it contribute to the electric signal collected by the amplifier. While the time development of the signal produced by the electrons can be approximated by a delta function, the time dependence of the ion signal is not negligible since their mobility is much lower than the electron mobility. According to Ref. [6] the contribution of the electron signal is only 15 % of the total signal ($\delta$ fraction = 0.15). Its time dependence is given by Eq. 1 to 3 for one electron-ion pair. The instant $t = 0 \ ns$ corresponds to the time when the electron is captured by the anode strip.

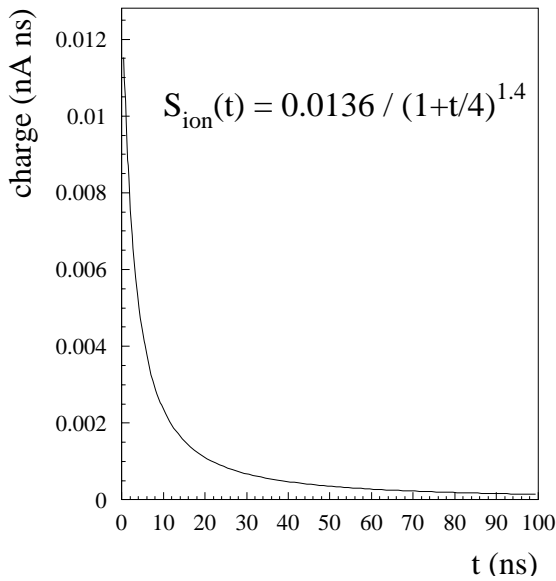$$S(t) = S_{\text{electron}}(t) + S_{\text{ion}}(t) \tag{1}$$

2

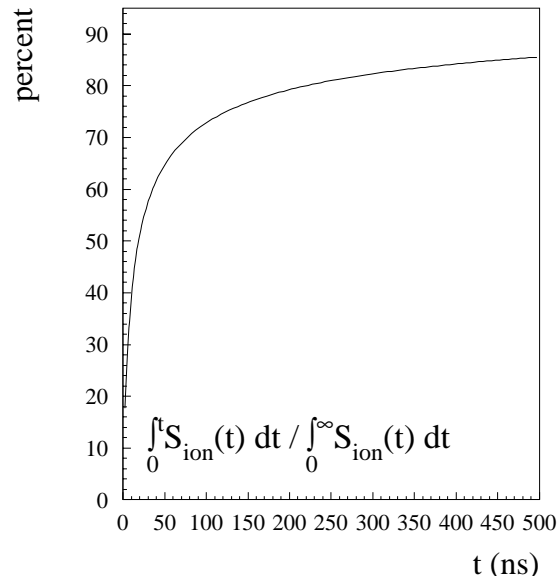Figure 1: Time function of the electric current induced on the anode strip by one ion in an avalanche.

Figure 2: Integrated charge, corresponding to the current function in Fig. 1, shown as a fraction of the total ion signal.

$$S_{\text{electron}}(t) = 0.15 \, e \, \delta(t) \tag{2}$$

$$S_{\text{ion}}(t) = 0.85 \, e \frac{m/t_0}{(1 + t/t_0)^{1+m}}, \qquad t > 0, \tag{3}$$

where $m$ and $t_0$ are estimated to be 0.4 and 4 ns respectively [6], so that

$$\int S(t) \, dt \;=\; e, \tag{4}$$

$e$ being the electron charge ($e = 0.16 \, nA \, ns$).

The ion drift contribute a relatively slow signal: the integration of $S_{\text{ion}}(t)$ (Fig. 1) over 25 ns, 50 ns and 1000 ns corresponds respectively to only 55%, 65% and 89% of the ion signal (see Fig. 2). The integration of the total signal $S(t)$ over 25 ns, 50 ns and 1000 ns amounts consequently to 61%, 70% and 91% of $S(t)$.

According to Ref. [6], this parameterization is an improvement on the one given in Ref. [4] since it reproduces better the tail of the current distribution, and it allows in addition to separate the electron and the ion contributions.

## 3 Response function of the shaping amplifier

It is planned to amplify the MSGC raw signal $S(t)$ with an APV of 50 ns shaping time $s_t$. This corresponds to a reponse function $R(t)$ with the following behaviour (Fig. 3):

$$R(t) = N \, R_1(t) \qquad \text{with} \qquad R_1(t) = \frac{t}{s_t} exp(\frac{-t}{s_t}), \quad t > 0, \tag{5}$$

where $N$ is the normalisation of $R(t)$ chosen in a way described in the next section.
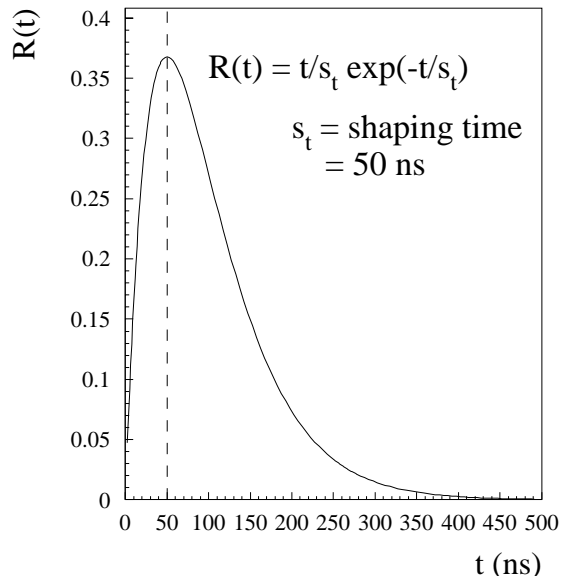
Figure 3: Shape of the amplifier response function.

# 4 Convoluted signal

For a single electron generating an avalanche at time $t = 0$, the amplitude $A(t)$ of the output signal of the MSGC+APV system is the convolution of the raw signal $S(t)$ (Eq. 1) with the amplifier response $R(t)$ (Eq. 5):

$$A(t) = S(t) \otimes R(t) = \int_{-\infty}^{t} S(x) \cdot R(t - x) \, dx \tag{6}$$

The normalisation of $R(t)$ should be chosen in such a way that the peak value of the convoluted signal $A(t)$ equals the integral of $S(t)$, i.e. the electron charge, in the case of an infinite shaping time $s_t = \infty$.

In the present analysis we have followed the approximation of Ref. [7] where a shaping time of 1000 ns is taken for the evaluation of the normalisation $N$:

$$N^{-1} = \text{maximum of} \int_{-\infty}^{t} S(x) \cdot R_1(t - x)|_{s_t = 1000ns} \, dx \tag{7}$$

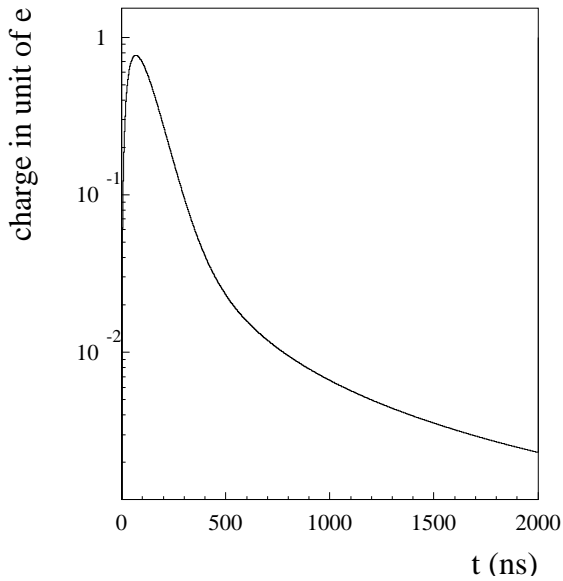The value of $N^{-1}$ found is 0.32828 and is used in the whole analysis.

Figure 4: Output signal of a MSGC+APV system for a single electron-ion pair input signal.
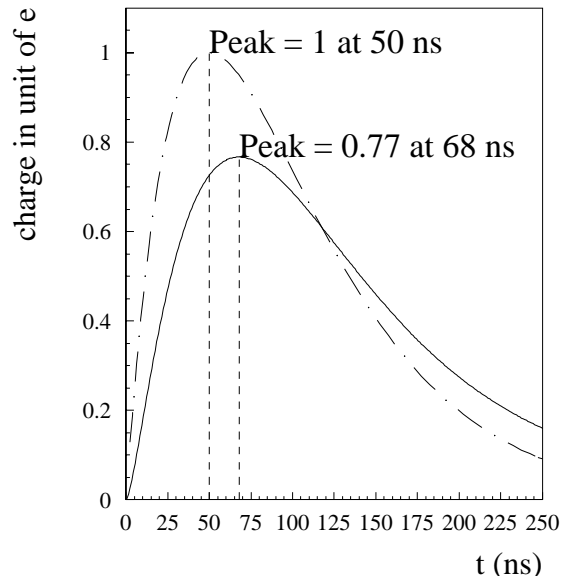
Figure 5: Comparison of the raw signal (full line) and a pure delta-function like signal (dotted line) after convolution with the amplifier response shape.

Figure 4 shows the convoluted signal $A(t)$ in logarithmic scale. In Fig. 5 the shape of $A(t)$ (full line) is compared with what would be the output signal for a pure delta-function signal (dotted line). The contribution of the ion part of the signal has two effects. First, because of its long lifetime, the maximum amplitude is reached at t = 68 ns, instead of the 50 ns of the amplifier shaping time. The second effect is called the *ballistic deficit*: because the shaping time is short with respect to the time development of the collected signal, 23% of the charge is lost. Note that there is more charge loss in case of avalanches occurring at time $t \neq 0$, as is it the case in an MSGC (see section 6). Figure 6 illustrates the dependence of the ballistic deficit on the shaping time of the amplifier.

The peak delay of the convoluted signal with respect to the shaping time is function of the ion signal shape, as is the peak amplitude. As can be seen in Fig. 7, the ballistic deficit decreases when the raw signal gets closer to a pure delta-function. This happens for a $\delta$ fraction getting closer to 1, or when either the constant $t_0$ decreases or $m$ increases. The ballistic deficit varies between 25% and 22.5% for the $\delta$ fraction going from 0.10 to 0.20, or for $t_0$ going from 4.7 down to 3.5, or for $m$ increasing from 0.37 to 0.43. Due to a lack of experimental data, it is not possible to have an estimate of the precision on these parameters.

## 5 Deconvolution of the signal

The CMS Tracker will record data at the frequency of one reading every $\Delta t$ = 25 ns, i.e. every bunch crossing. It is necessary to keep in memory each reading until a level 1 trigger is produced for a given bunch crossing occurring at time $T_{trigger}$. Since the MSGC output signal $A(t)$ lasts for about 10 bunch crossings, it needs to be reshaped in order to reduce its length in time. In the present analysis the procedure implemented consists in deconvoluting the signals as proposed in Ref. [8]. The values $r(t)$ read at each channel at time $t_1 = T_{trigger}$, $t_2 = T_{trigger} + \Delta t$ and $t_3 = T_{trigger} + 2\Delta t$ are weighted by using predefined weights to yield a deconvoluted amplitude $D(T_{trigger})$ as described below.

### 5.1 Deconvoluted signal

The deconvoluted signal $D(t)$ corresponding to a given trigger time $T_{trigger}$ is given by:

$$D(T_{trigger}) = w_1 \, r(T_{trigger}) \; + \; w_2 \, r(T_{trigger} + \Delta t) \; + \; w_3 \, r(T_{trigger} + 2\Delta t) \tag{8}$$

where $w_1$, $w_2$ and $w_3$ represent the weights, $r(t)$ are the reading values at time $t$, and $\Delta t$ is 25 ns as mentioned before.
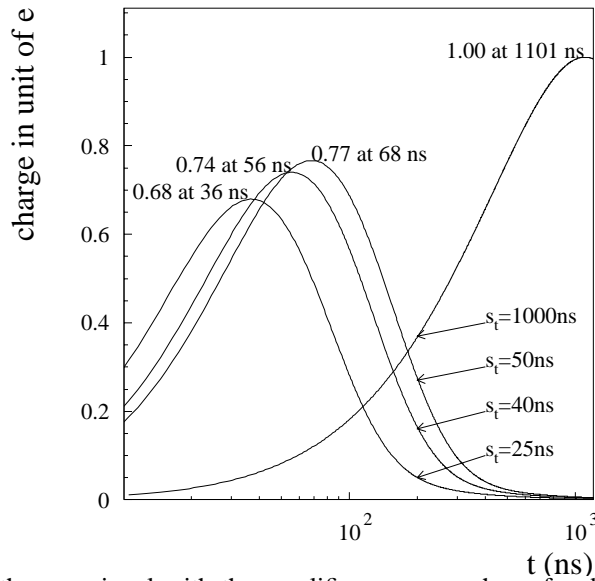
Figure 6: Convolution of the raw signal with the amplifier response shape for different shaping times $s_t$. By construction, the peak value of the curve $s_t = 1000$ ns is equal to 1.

The weights have to be chosen in such a way that:

- $D(T_{trigger})$ amounts to the charge collected by the APV when a signal actually started at time $= T_{trigger}$. This requirement assumes a low probability that there be signals on the same readout channel at three consecutive bunch crossings. If the probability is not negligible, the signal of the consecutive events should be summed before deconvolution, which is not the case in the present simulation in ORCA.

- $D(T_{trigger})$ penalises early and late signals. This requirement competes with good detection efficiency since primary ionisation electrons drift for 0 to 55 ns, i.e. more than two bunch crossings, before producing an avalanche. This point is detailed in section 6.

The weight values proposed in Ref. [8] are:

$$w_1 = -1.202, \qquad w_2 = 0.172, \qquad w_3 = 0.858. \tag{9}$$

As explained in [9], the deconvolution operation is equivalent to reshaping the signal with a shorter time constant, which implies that the series noise is expected to increase. In the present case, the series noise factor (SNF) is estimated to be:

$$SNF = 1.474. \tag{10}$$

These weights have been evaluated as being optimal for fulfilling the upper two requirements. However the weighted sum of Eq. 8 amounts to 1 for a pure delta-function signal, but is 0.70 instead of 0.77 ($= 1 - 0.23$) if the ion contribution is taken into account as described in the previous sections (see Fig. 5). This will result in a further 9% signal loss which could be avoided by adapting the weights accordingly. However, if the weights were increased by 9% such that there would be no further signal loss, so would be the Series Noise Factor, and the Signal to Noise ratio would not change. In the following the weights given in Eq. 9 and recommended in [8] are used.

For an avalanche occurring at time $t = T_{trigger} + dt$ with a delay $dt$ positive or negative respect to the trigger time, the deconvoluted signal $D(dt)$ is ($T_{trigger} = 0$):

$$D(dt) = w_1 \, A(-dt) + w_2 \, A(-dt + \Delta t) + w_3 \, A(-dt + 2\Delta t) \tag{11}$$

where $A(t)$ is defined in Eq. 6 and is equal to zero for negative values of $t$. Clearly, charges collected later than $2\Delta t$ after the trigger time do not contribute to the corresponding bunch crossing signal. As seen in Fig. 8, the deconvoluted amplitude is negative for signal starting at least 40 ns before the trigger time. This implies that crosstalk pulses can fake signals: crosstalk pulses have the same shape as the signal but with negative amplitudes;
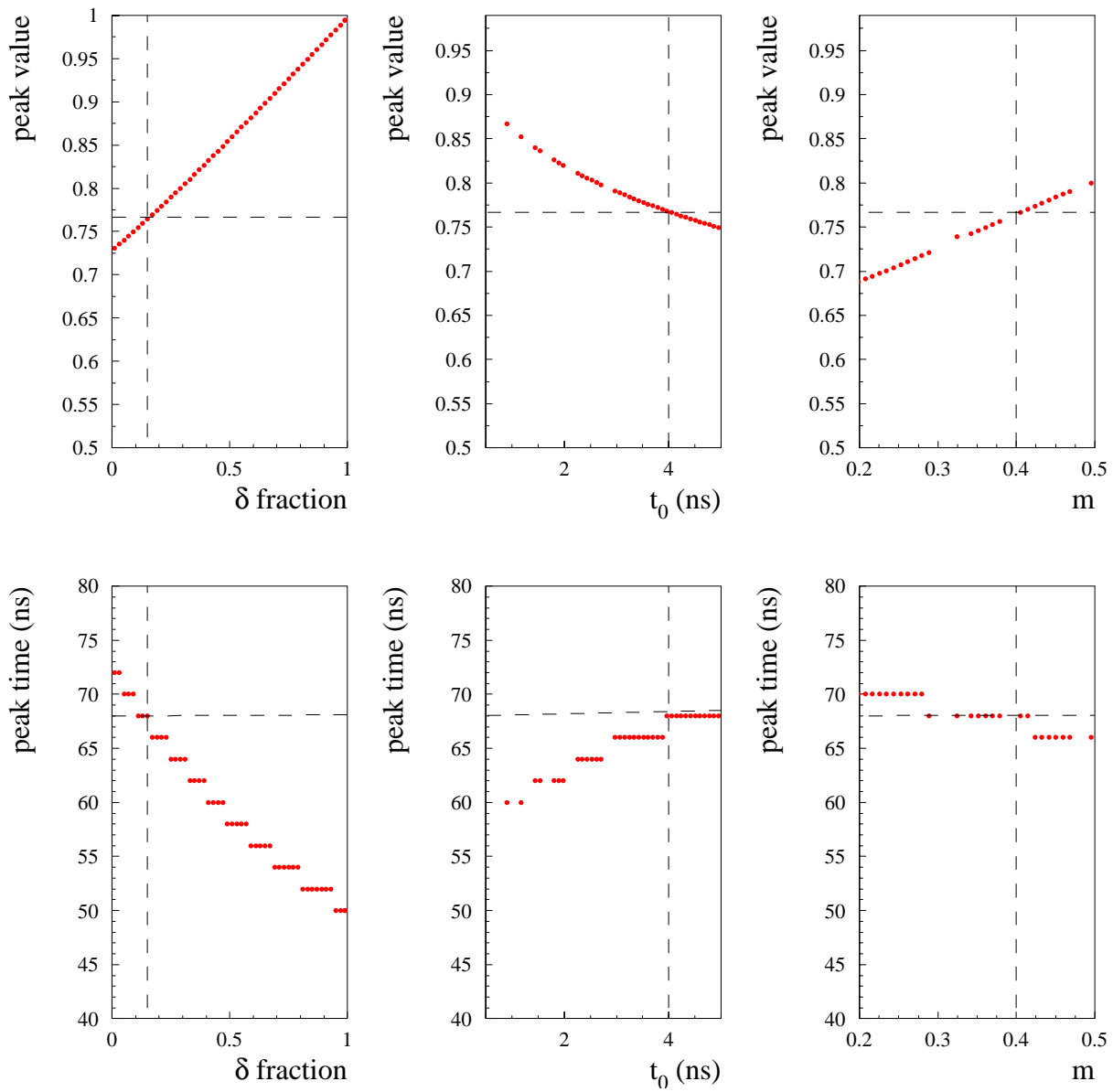
6

Figure 7: Peak value and time of the convoluted signal for different values of the electron contribution to the total raw signal ($\delta$ fraction), the constant $t_0$ and the constant $m$ of the ion signal shape. In each case, the parameters which are not being varied have the value used in this simulation ($\delta = 0.15$, $t_0 = 4$ ns, $m = 0.4$). The segmentation of the curves is due to the use of integer time values.

they are deconvoluted in the same way as the signal. Note that $D(dt)$ becomes zero for $dt = -\infty$ since $A(t)$ vanishes only for $t = +\infty$. The value of $D(dt)$ at $dt = -500$ ns is $-0.008$.

Figure 9 shows that the deconvolution slightly favours positive delay times for $|dt| < 50$ ns.

# 6 Particle signal in a CMS MSGC

The total deconvoluted signal collected by an MSGC strip for the trigger happening a $t = T_{trigger}$ is the sum of the contribution $D(dt_i)$ of all avalanches which occurred not later than $2\Delta t$ after $T_{trigger}$:

$$D_{strip}(T_{trigger}) = \sum_{\text{avalanches } i} g_i \cdot D(dt_i), \quad -\infty < dt_i < T_{trigger} + 2\Delta t \tag{12}$$
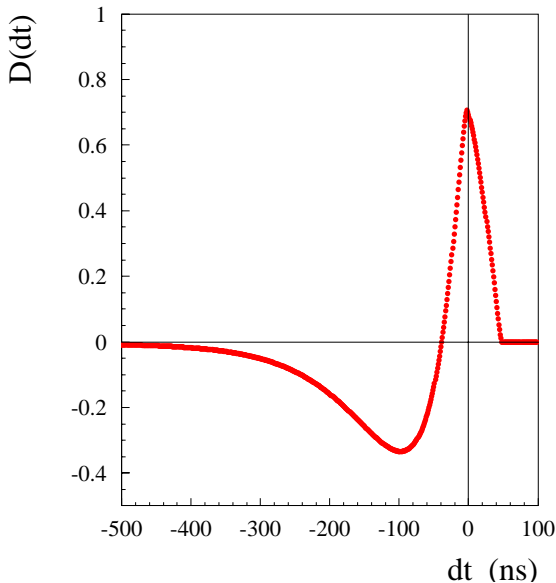
Figure 8: Deconvoluted amplitude for one avalanche signal, as a function of the signal delay dt with respect to the trigger time (dt is positive for signal starting later that the trigger time).
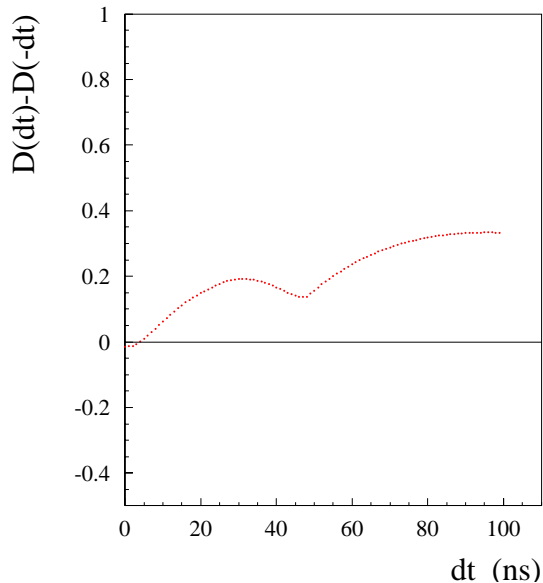
Figure 9: Time asymmetry of the deconvoluted amplitude.

For each individual avalanche $i$, $g_i$ is the gain and $dt_i$ amounts to the time of flight of the incident particle before it enters the chamber, plus the drift time of the primary ionisation electron until it generates an avalanche. For the 3 mm thick CMS MSGC's, the drift time is between 0 and 55 ns (more than two bunch crossings). The deconvolution logic has thus to be tuned by an offset corresponding to the mean drift time (offset = 55ns/2): Eq. 12 is replaced by:

$$D_{strip}(T_{trigger}) = \sum_{\text{avalanches } i} g_i \cdot D(dt_i - \text{offset}), \quad -\infty < dt_i < T_{trigger} + 2\Delta t \qquad (13)$$

In the full simulation of the CMS Tracker, an additional offset should be applied to take into account the distance of the chamber with respect to the interaction point: the time of flight of a high pT particle created at $T_{trigger}$ is a few nanoseconds. This introduce a systematic effect on the result of the deconvolution. In the analysis of the occupancy presented in Section 8, the tuning of the delay seen by the different detectors has not been implemented.

# 7   Effect of deconvolution

## 7.1   Signal to Noise ratio

A sample of hits produced by single minimum ionizing particles (mip's) is simulated with a standalone program (i.e. single chamber geometry) using the following specifications: single 0.6 GeV $\pi^-$'s are simulated crossing at a random point the 3 mm gas layer of Ne/DME (30/70). For an incidence angle of zero with respect to the strip plane, an average of about 33 electron-ion pairs are formed along the track in the gas with a peak value of 20 (see Fig. 10).

The avalanches produced by these electrons correspond to a mean gain factor of 2500 in the present simulation. The gain fluctuations are simulated according to a Polya function, as seen in Fig. 11. A noise of 1250 electrons is generated. Gain and noise values are the ones quoted in the TDR [1] (Chapter 7.10.2). Gas diffusion is simulated with a coefficient of 0.016 cm/cm$^{1/2}$. A 4T magnetic field is applied in the direction parallel to the strip direction. This corresponds to the CMS Barrel configuration, but without tilting of the chamber. The drift direction has an angle of 14 degrees with respect to the normal direction. The detector pitch is 0.02 cm. Charge clusters are reconstructed by looking for sets of adjacent strips with signal larger than 1.8 times the noise. It is required that at least one strip signal per set has a charge larger than 3.5 times the noise. No requirement is done on the total cluster charge. The factor for charge conversion into ADC counts used here is 80 electrons per ADC count.
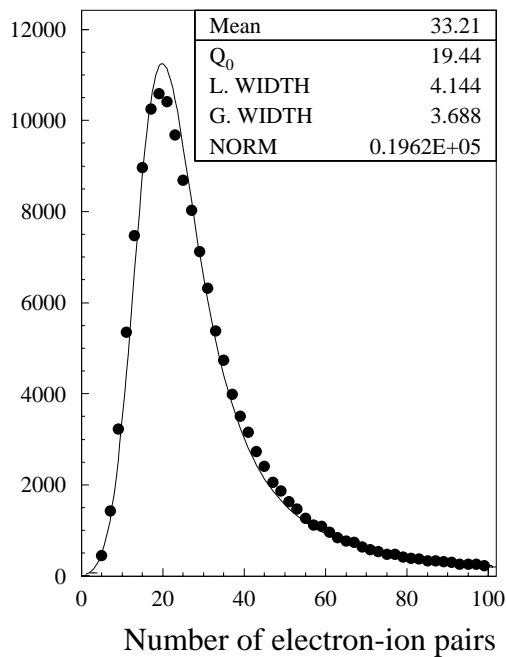
| Mean | 33.21 |
|---|---|
| $Q_0$ | 19.44 |
| L. WIDTH | 4.144 |
| G. WIDTH | 3.688 |
| NORM | 0.1962E+05 |

Figure 10: Distribution of the number of primary and secondary electron-ion pairs produced by a mip (0.6 GeV $\pi^-$) at normal incidence in 3 mm of 30% Ne - 70% DME gas mixture, B=4T.
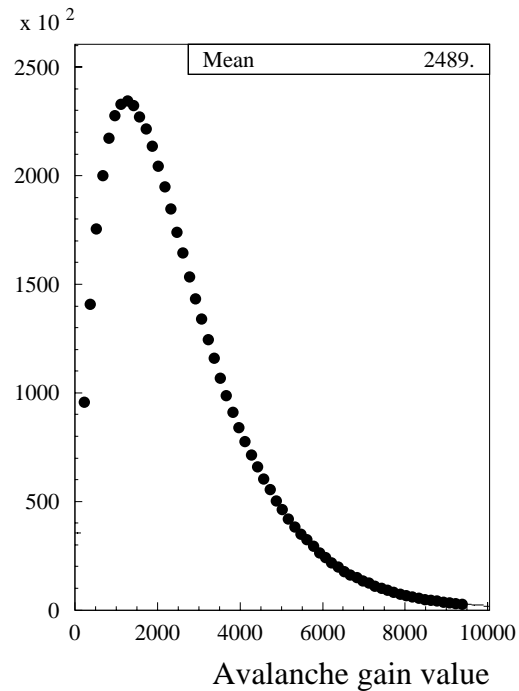


| Mean | 2489. |
|---|---|

Figure 11: Simulated Polya avalanche gain distribution with mean value set to 2500.

Figures 12 and 15 show the cluster charge obtained in an "ideal" case (i.e. no signal loss due to ballistic deficit, no shaper, no electronic effect, no deconvolution) and in deconvolution mode respectively. When more than one cluster was reconstructed the one closest to the particle impact point is considered. Figure 14 shows that the sum of the ballistic deficit and the deconvolution process induces a signal loss of 50%. This is compatible with the expected 0.54 signal loss quoted in the TDR [1] (Chapter 7.10.3).

The Signal to Noise ratio is evaluated as the ratio between the most probable cluster charge and the noise of one strip. The value of S/N depends on the angle between the track and the electron drift directions: when that angle increases the charge is collected by more strips. Consequently the probability for the charge collection to be below the clustering threshold increases, and part of the charge maybe lost at reconstruction time. Figures 13 and 16 show the values of S/N as a function of the track incidence angle, in an "ideal" case and in deconvolution mode, respectively. As expected, the maximum values are found for the track direction corresponding to the drift direction; they are S/N = 36 in the "ideal" case and S/N = 12 in deconvolution mode. The S/N decrease when applying deconvolution is compatible with the expected 0.5 signal loss and the increase in effective noise of 1.474 (see Eq. 10). The fit results used in these last two plots are shown in Fig. 36 and 37 at the end of this paper.

In Fig. 17 the reconstruction efficiency is given as a function of the time of arrival of the particle to the chamber. No noise has been generated to produce that figure. A simulated hit is considered as being reconstructed if it has contributed the equivalent of at least 1/2 ADC count to the charge of at least one cluster. The effect of the crosstalk mentioned in section 5.1 is visible for negative values of the time.

## 7.2   New clustering algorithm

Clustering algorithms can be designed, that give improved efficiency for inclined tracks. In the following, a study is shown, where clusters are defined applying thresholds of 1.4 and 4.0 times the noise, for the individual strip signals and the total cluster charge respectively. No requirement is set on the strip with the maximum charge. This clustering increases the average number of pure noise clusters per detector from 0.12 to 1 for 512 strips detectors, and increases the effect of crosstalk, but it improves the hit efficiency from 87% to 93% (see Fig. 17 and  20) and it allows to get a non-truncated cluster charge distribution at low charge values (see Fig. 18).
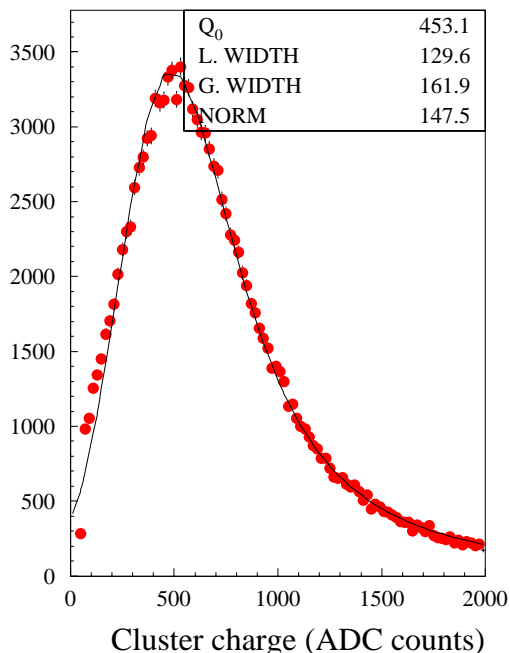
| $Q_0$ | 453.1 |
|---|---|
| L. WIDTH | 129.6 |
| G. WIDTH | 161.9 |
| NORM | 147.5 |

Figure 12: Simulated cluster charge for mip's (0.6 GeV $\pi^-$) at normal incidence, in case of no charge loss but for clustering effects, B=4T, with clustering thresholds 1.8-3.5-0.
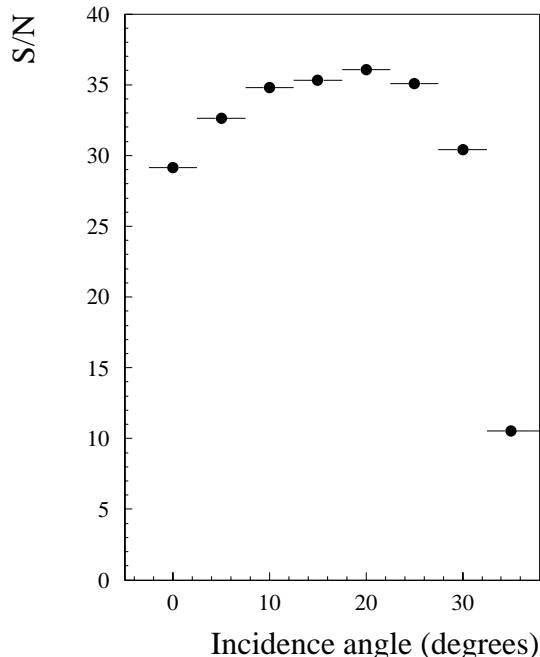
Figure 13: S/N ratio for mip's (0.6 GeV $\pi^-$) as a function of the particle incidence angle, in case of no charge loss but for clustering effects, B=4T, with clustering thresholds 1.8-3.5-0.

Figure 22 corresponds to Fig. 20 but with noise generated "on-time", i.e. at the trigger time. The non-negligible probability to find a cluster associated to a track for negative impact times is due to the presence of positive crosstalk contribution, in addition to the fact that crosstalk occurs on a block of 32 strips. The reconstruction is sensitive to an effective number of 3.1 bunch crossings including the trigger one. The effect of the asymmetry of the deconvolution function with respect to positive et negative times (see Fig. 9) is visible in Fig. 21.

Figure 23 shows the hit reconstruction efficiency as a function of the particle incidence angle. As said previously, a simulated hit is considered as being reconstructed if it has contributed the equivalent of at least 1/2 ADC count to the charge of at least one cluster.

Figures 24 and 25 show respectively the cluster multiplicity and the cluster size as a function of the particle incidence angle. In the counting of reconstructed clusters, only clusters where at least the equivalent charge of 1/2 ADC count is contributed by the particle, are considered.

Figure 26 shows the hit resolution. When more than one cluster was reconstructed, only the one closest to the particle impact point was considered. The cluster multiplicity is minimum and constant within 15 degrees around the drift direction. Clusters then split as the charge tends to be shared on more than 4 strips. The hit resolution increases with the angle between the track direction and the drift direction. It is at best 30 $\mu$m.

# 8 MSGC occupancy in CMS

The MSGC occupancy results presented in the TDR [1] are obtained with a Monte Carlo analysis which does not include a detailed simulation of the signal deconvolution. It uses an effective gain of 2170 and an effective noise of 1875 electrons, which correspond to a S/N ratio of 18. In order to fake the contribution of early signals, 48 minimum bias events are cumulated with Poisson statistical fluctuations. In the case of the ORCA simulation, values of 2500 and 1250 electrons are used for the gain and the noise respectively. This corresponds to a S/N ratio of 12 for mips as shown in section 7.1. The amount of tracks processed per trigger bunch crossing corresponds to an average of 24 minimum bias events per bunch crossing (with Poisson fluctuations), taking into account 10 bunch crossings before the trigger and 2 after. In view of the result obtained in section 7.1 indicating a sensitivity
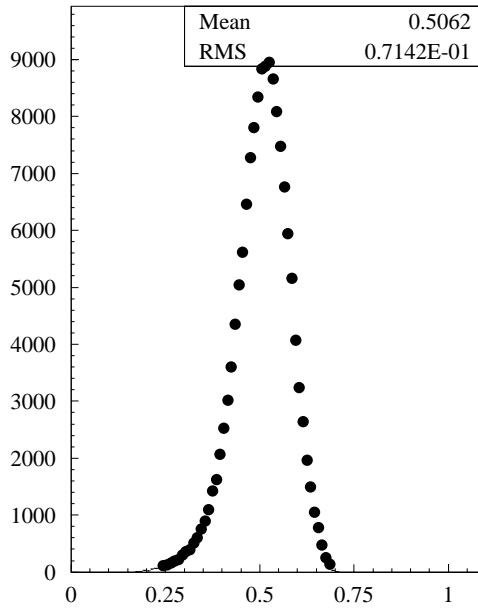
| Mean | 0.5062 |
| RMS | 0.7142E-01 |

Figure 14: Signal loss due to ballistic deficit and deconvolution for mip's (0.6 GeV $\pi^-$) at normal incidence in a CMS MSGC, B=4T (simulation).

of the deconvolution process to 3.1 bunch crossings, the factor 2 used in the TDR (the cumulation of 48 minimum bias events) is expected to be under-estimated.

In the following figures, results are shown for both the TDR approximation (black circles) and the ORCA detailed simulation (red stars). In both cases, "on-time" noise is simulated in all detectors (i.e. even if there was no particle impact).

Figure 27 shows the average number of track impact per detector. As expected it is higher for the ORCA simulation than for the TDR, since in the first case an average of 312 minimum bias events are analysed, and only 48 in the second case. The same effect is seen in Fig. 28 for the percentage of hit detectors. The number of clusters non-associated to a particle (Fig. 35) larger when using the ORCA simulation because of the crosstalk effect described in section 5.1.

Both the detector occupancy estimates are found to be larger in presence of deconvolution by a factor of about 50%. (see Fig. 29 and 30).

Figures 31, 32 33, and 34 give the cluster splitting rates as a function of $p_T$ for single minimum bias events (no pile-up), for the TDR and the ORCA analysis respectively. The discontinuity of the curve in Fig. 31 for particles with $p_T$ <0.6 GeV is explained by the fact that this is the limit energy for the particle to reach the last MSGC layers. Consequently, at these energies, particles are mostly secondaries for which the incidence angle and $p_T$ are no more correlated.

# 9   Conclusions

We have simulated the deconvolution logic foreseen to be applied on the CMS MSGC signals. The simulation has been performed with the ORCA software where the pile-up of off-time bunch-crossing events is properly handled. This study is based on the available information concerning the model of raw signal generation, the amplifier shaping and the normalisation of the convoluted signal. No data were available at the time when this study was performed, to validate and tune our modeling. The largest uncertainty on the charge readout model is contributed by the convoluted signal normalisation.

Another relevant unknown in our model is the noise correlation at subsequent readings. The noise has been

generated according to a Gaussian distribution at each event. Also the effect of the pedestal substraction has not been simulated. Regarding these simplifications, it is expected that in the real CMS conditions, the detector performance would be degraded with respect to the estimates obtained here.

Within these assumptions, with have estimated that the signal shaping and deconvolution produces a signal loss of 50%, yielding a Signal to Noise ratio of 13 for minimum ionising particles at normal incidence. It has been stressed that the deconvolution weight factors could probably be improved for recovering about 9% of the signal. A hit reconstruction of 93% was obtained for on-time particles, with a total sensitivity to 3.1 bunch-crossings, included the trigger one. It has been shown that the signal deconvolution results in a positive crosstalk effect for early particles, which increases significantly the detector occupancy.

# References

[1] **CERN LHCC/98-6, CMS TDR 5**, CMS Collaboration, *"CMS: The Tracker Project: Technical Design Report"*

[2] **CMS Internal Note, CMS/IN 99/35**, D.Stickland, *"CMS Reconstruction Software: The ORCA project"*

[3] **CMS Internal Note, CMS/IN 2000/016** with reference to [4] and to [5], V.Lefébure, *"MSGC response simulation in ORCA"*

[4] **INFN PI/AE-94/02**, R.Bellazzini and M.A.Spezziga, *"Electric field, avalanche growth and signal development in Micro-Strip Gas Chamber and Micro-Gap Chamber"*

[5] **NATO-ASI Series, B:Physics Vol.365, Ed. Thomas Ferbel, 1997** *Techniques and Concepts of HEP*

[6] **Thesis of Mario Spezziga**, Mario Spezziga, *thesis in preparation with reference to [5].*

[7] **CMS NOTE/97-105**, F.G. Sciacca, *"Impact of Fast Shaping at the Front-end on Signals from Micro Strip Gas Chambers"*

[8] **CMS NOTE/97-021**, F.G. Sciacca, *"Definition of the Front-end Signal Processing Algorithm for MSGC's in CMS"*

[9] **CMS THESIS/99-082**, F.G. Sciacca, *"Analogue Readout and Signal Processing for Micro Strip Gas Chambers of the Compact Muon Solenoid at LHC"*

| Q_0 | 193.9 |
|---|---|
| L. WIDTH | 62.38 |
| G. WIDTH | 138.6 |
| NORM | 364.6 |

Cluster charge (ADC counts)
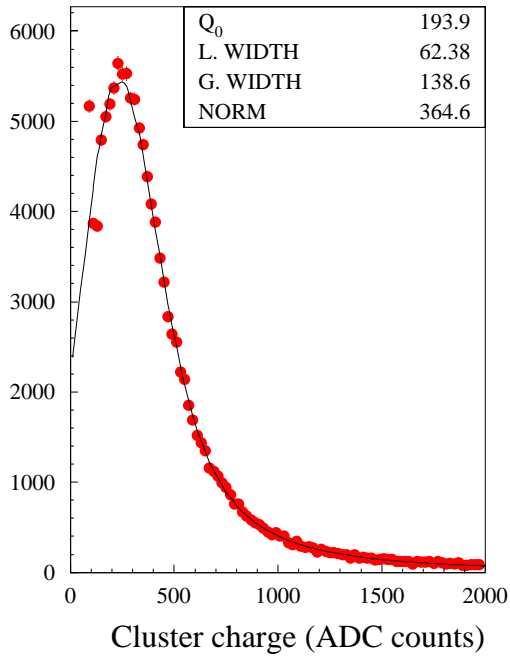
Figure 15: Simulated cluster charge for mip's (0.6 GeV $\pi^-$) at normal incidence, in deconvolution mode, B=4T, with clustering thresholds 1.8-3.5-0.
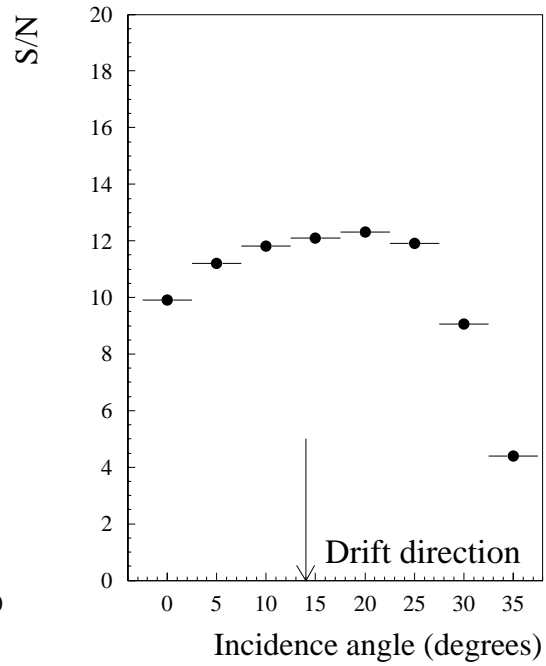
Incidence angle (degrees)
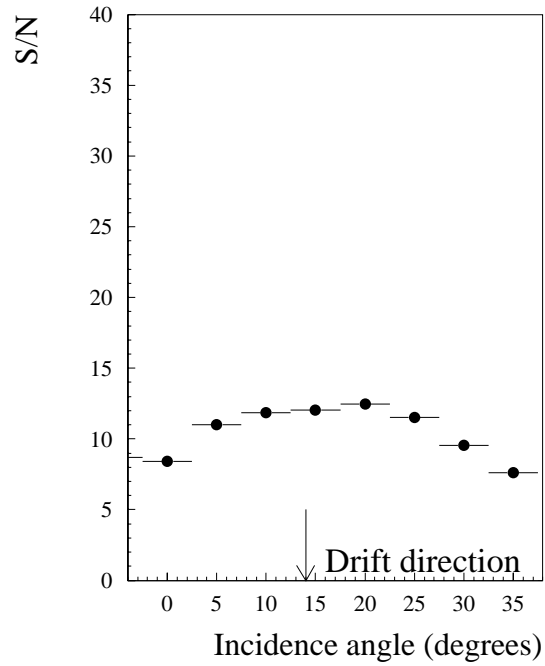
Figure 16: S/N ratio for mip's (0.6 GeV $\pi^-$) as a function of the particle incidence angle, in deconvolution mode, B=4T, with clustering thresholds 1.8-3.5-0.
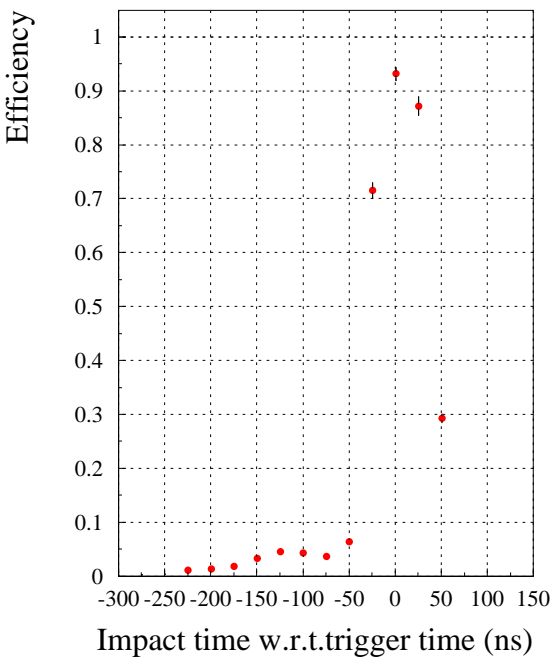
Impact time w.r.t.trigger time (ns)
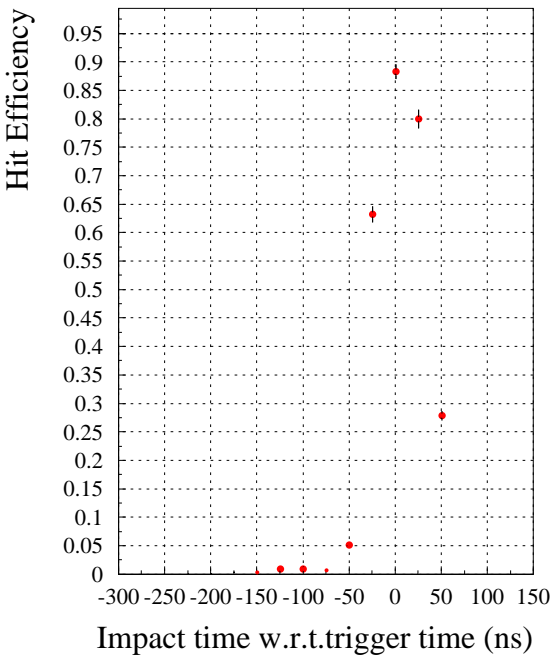
Figure 17: Reconstruction efficiency as a function of impact time for mip's (0.6 GeV $\pi^-$) crossing an MSGC chamber at normal incidence, B=4T, with clustering thresholds 1.8-3.5-0. No noise has been simulated.

14

| | |
|---|---|
| $Q_0$ | 239.5 |
| L. WIDTH | 68.27 |
| G. WIDTH | 85.33 |
| NORM | 489.2 |
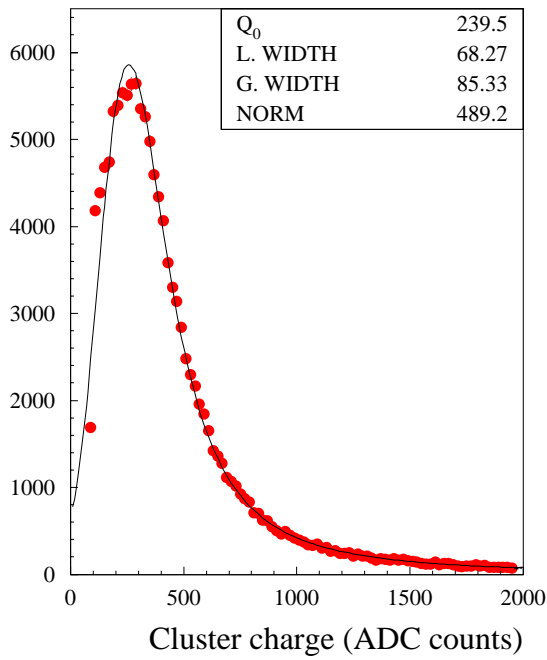
Figure 18: Simulated cluster charge for mip's (0.6 GeV $\pi^-$) at normal incidence, in deconvolution mode, B=4T, with clustering thresholds 1.4-0.-4.

Figure 19: S/N ratio for mip's (0.6 GeV $\pi^-$) as a function of the particle incidence angle, in deconvolution mode, B=4T, with clustering thresholds 1.4-0.-4

Figure 20: Hit reconstruction efficiency as a function of impact time for mip's (0.6 GeV $\pi^-$) crossing an MSGC chamber at normal incidence, B=4T, with clustering thresholds 1.4-0.-4. No noise has been simulated.
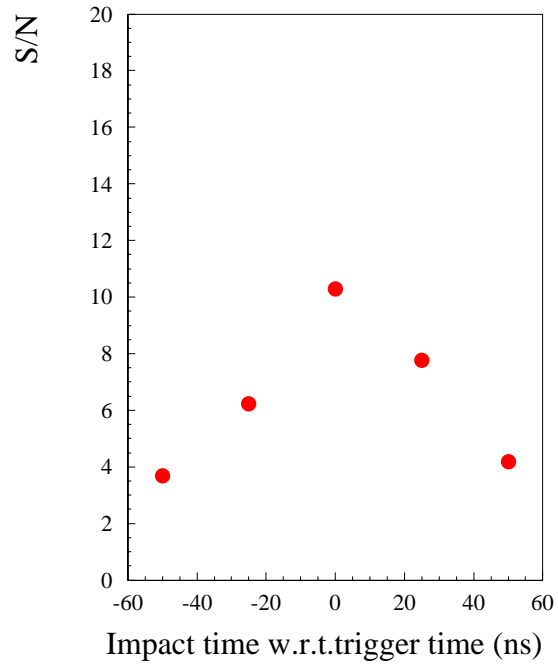
Figure 21: Signal to Noise ratio as a function of impact time for mip's (0.6 GeV $\pi^-$) crossing an MSGC chamber at normal incidence, B=4T, with clustering thresholds 1.4-0.-4. No noise has been simulated.

15
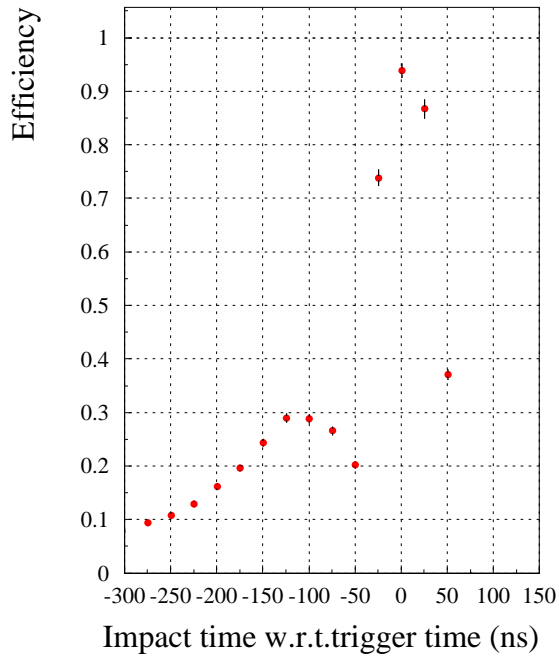
Figure 22: Hit reconstruction efficiency as a function of impact time for mip's (0.6 GeV $\pi^-$) crossing an MSGC chamber at normal incidence, B=4T, with clustering thresholds 1.4-0.-4. On-time noise has been simulated.
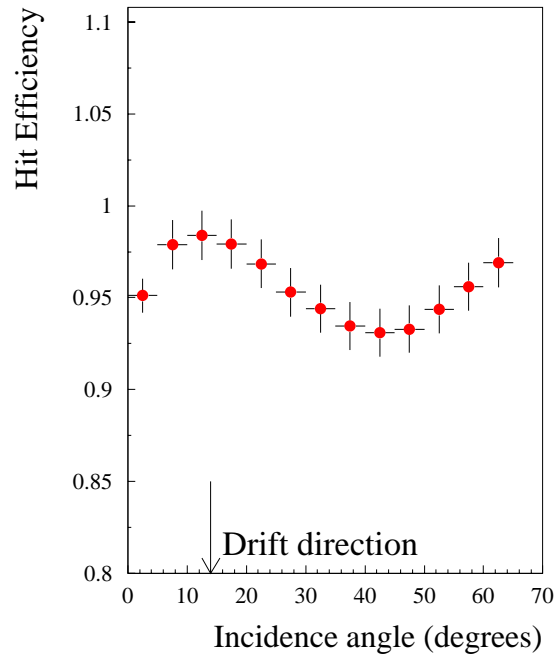


Figure 23: Hit reconstruction efficiency as a function of the particle incidence angle for mip's (0.6 GeV $\pi^-$), B=4T, with clustering thresholds 1.4-0.-4. On-time noise has been simulated.
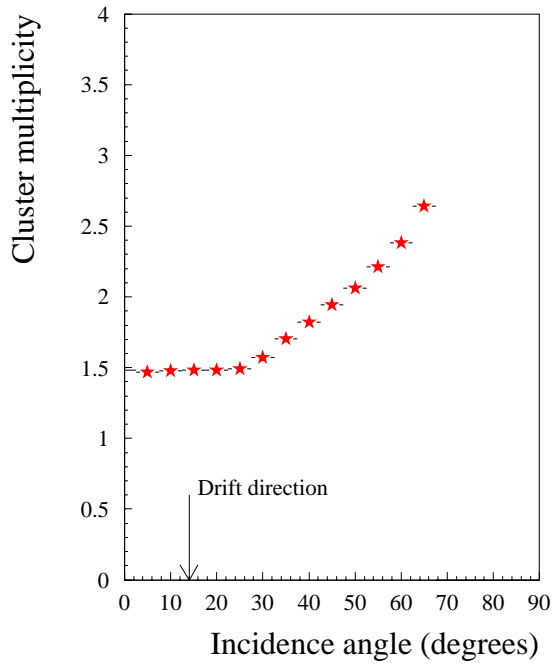
Figure 24: Cluster multiplicity in an MSGC with 0.02 cm pitch, as a function of the particle incidence angle, for mip's (0.6 GeV $\pi^-$). Deconvolution mode, with clustering thresholds 1.4-0.-4, B=4T.
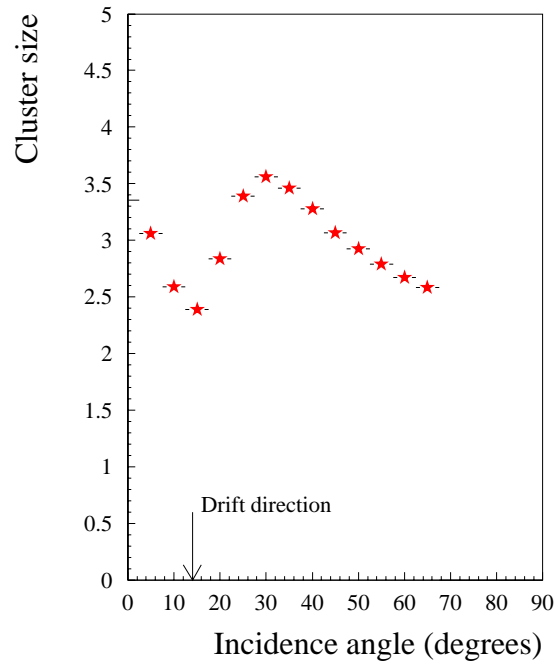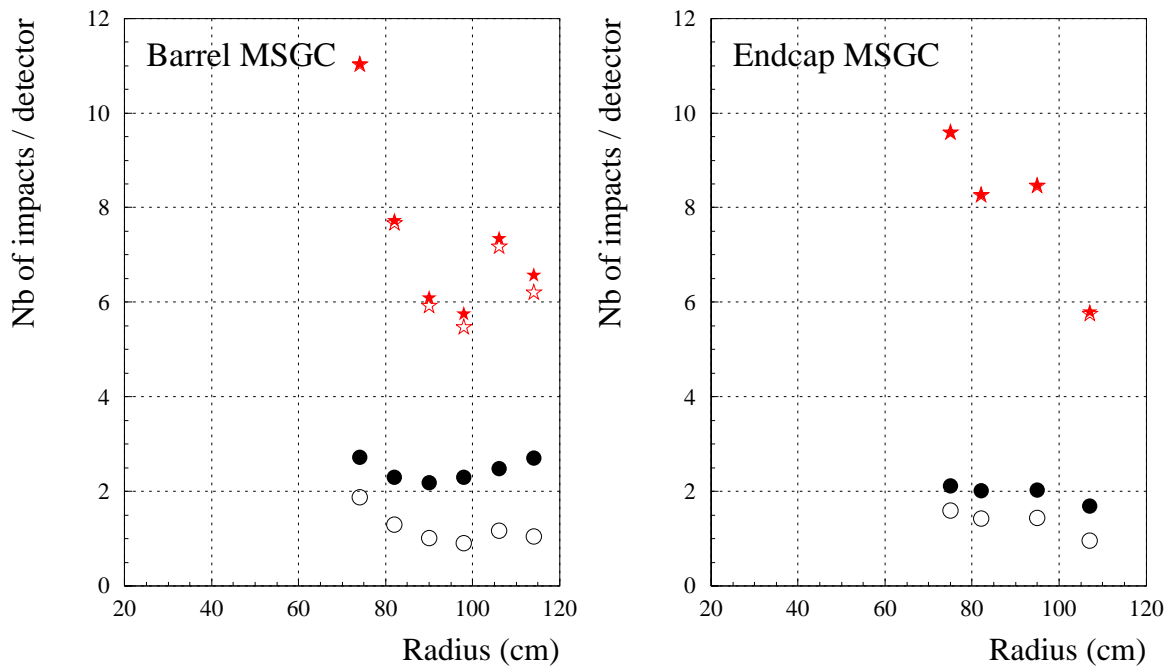


Figure 25: Cluster size in an MSGC with 0.02 cm pitch, as a function of the particle incidence angle, for mip's (0.6 GeV $\pi^-$). Deconvolution mode, with clustering thresholds 1.4-0.-4, B=4T.
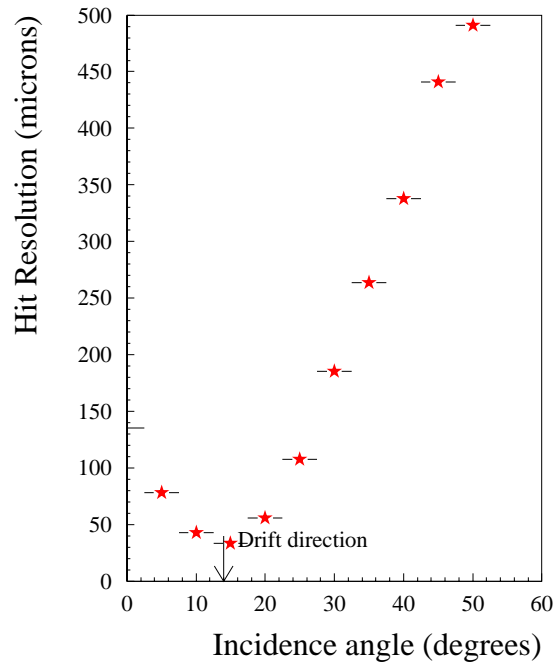


Figure 26: MSGC position resolution as a function of the particle incidence angle, for mip's (0.6 GeV $\pi^-$). Deconvolution mode, with clustering thresholds 1.4-0.-4, B=4T.

Figure 27: Average number of tracks per barrel (left) and endcap (right) module in high luminosity minimum bias events as a function of detector radius. Average values are calculated considering all detectors (open symbols) or exclusively detectors crossed by at least one track (close symbols). (Circles = TDR approximation; stars = ORCA detailed simulation, with pile-up of 10 bunch-crossings before the trigger event and 2 after.)
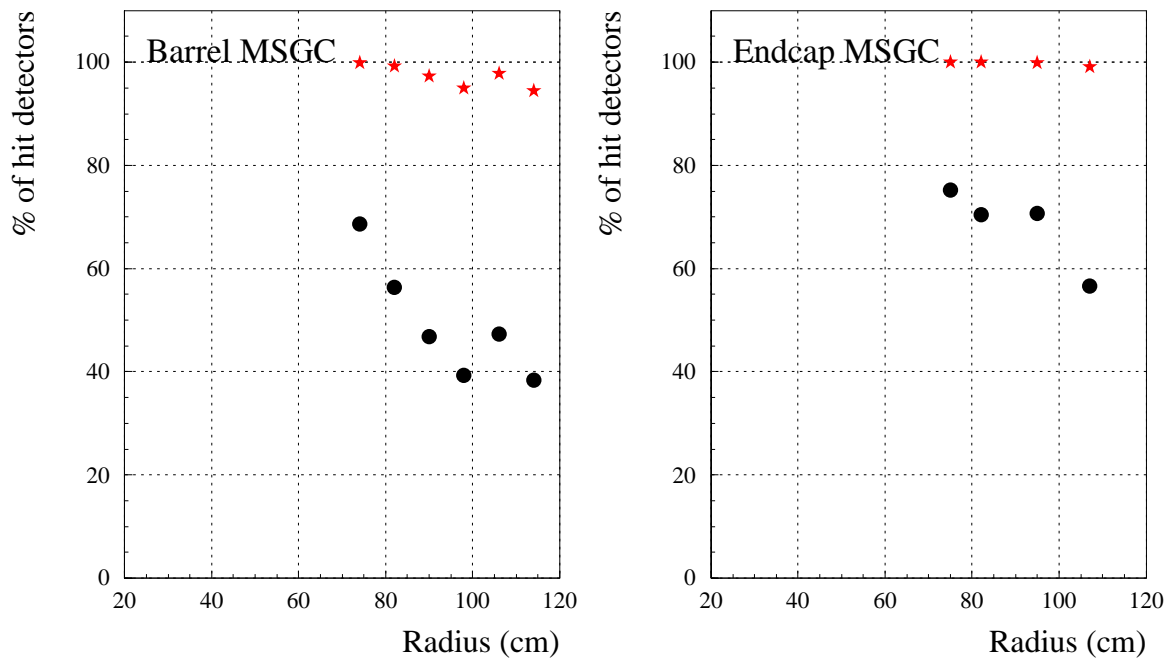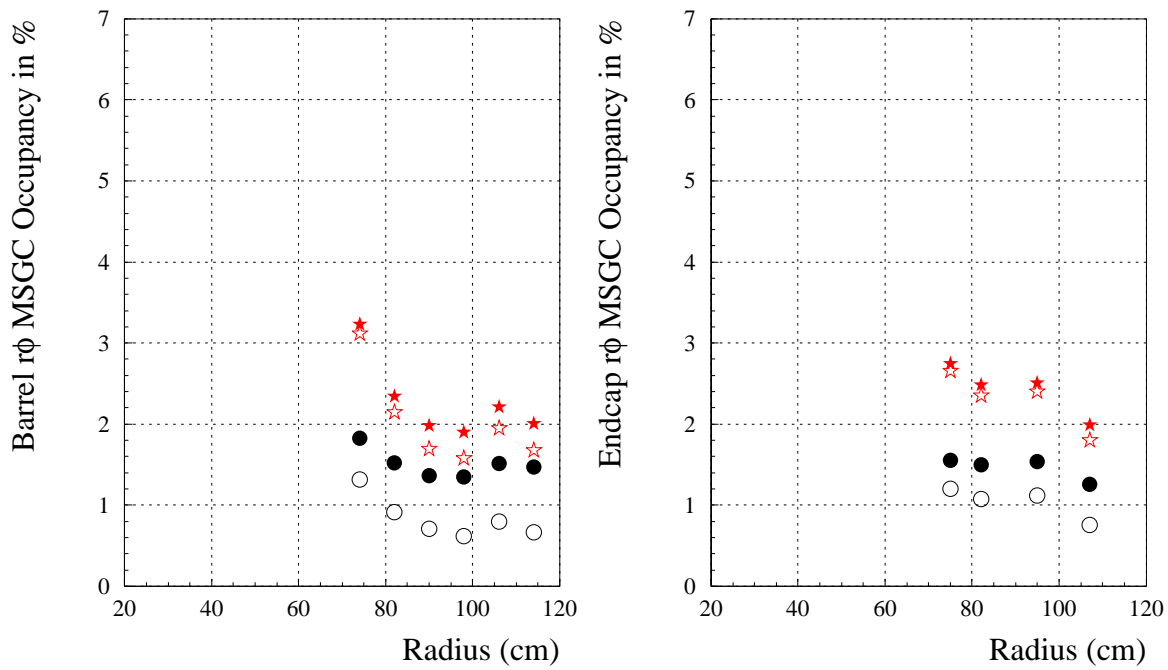


Figure 28: Percentage of barrel (left) and endcap (right) detectors crossed by tracks in high luminosity minimum bias events as a function of detector radius. (Circles = TDR approximation; stars = ORCA detailed simulation, with pile-up of 10 bunch-crossings before the trigger event and 2 after.)

Figure 29: Occupancy in rφ barrel (left) and endcap (right) detectors. Average values are calculated considering all detectors (open symbols) or exclusively detectors crossed by at least one track (close symbols). (Circles = TDR approximation; stars = ORCA detailed simulation, with pile-up of 10 bunch-crossings before the trigger event and 2 after.)
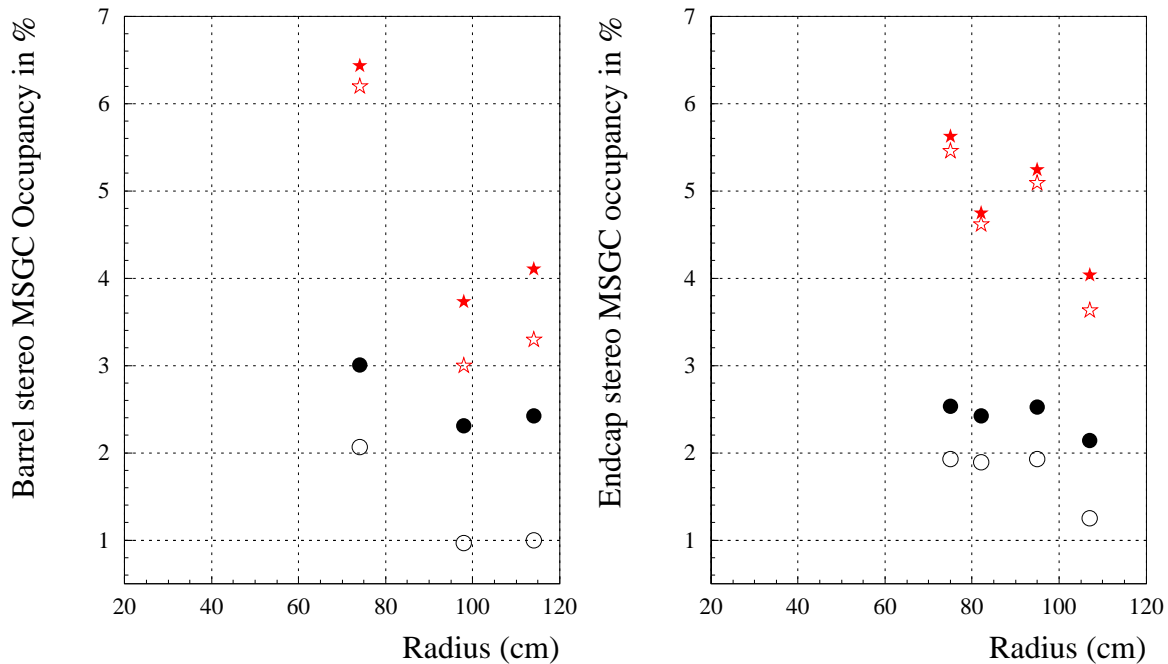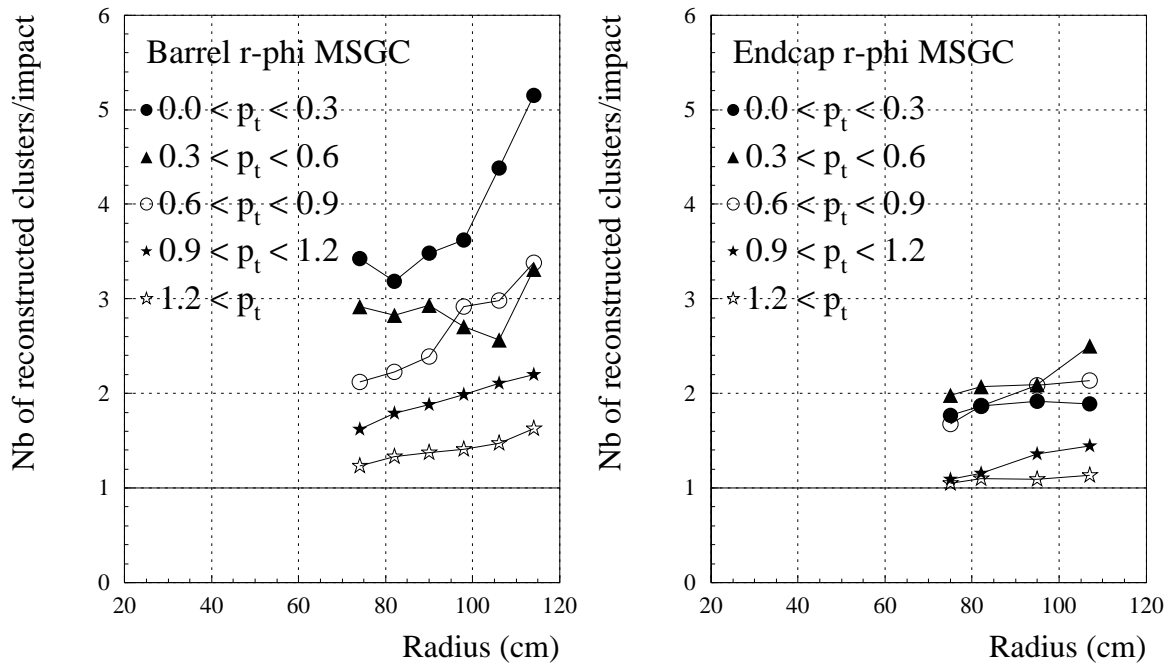


Figure 30: Occupancy in stereo barrel (left) and endcap (right) detectors. Average values are calculated considering all detectors (open symbols) or exclusively detectors crossed by at least one track (close symbols). (Circles = TDR approximation; stars = ORCA detailed simulation, with pile-up of 10 bunch-crossings before the trigger event and 2 after.)

Figure 31: Cluster splitting rate in the r$\phi$ barrel (left) and endcap (right) detectors as a function of the detector radius for different ranges of $p_T$ (GeV). (TDR approximation.)
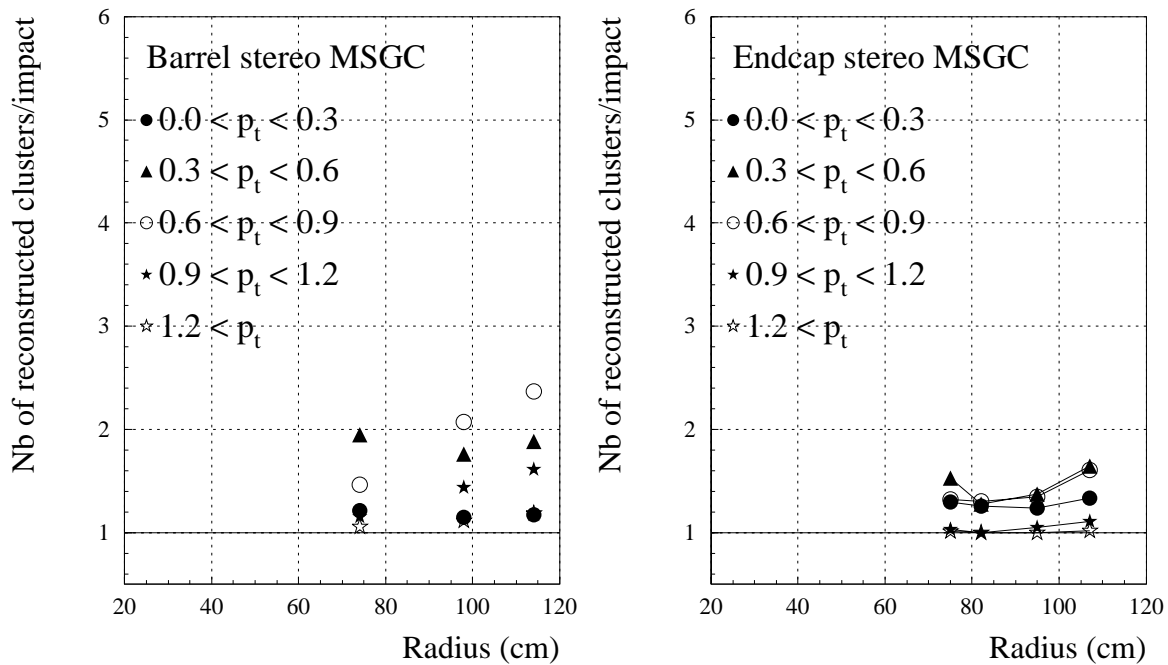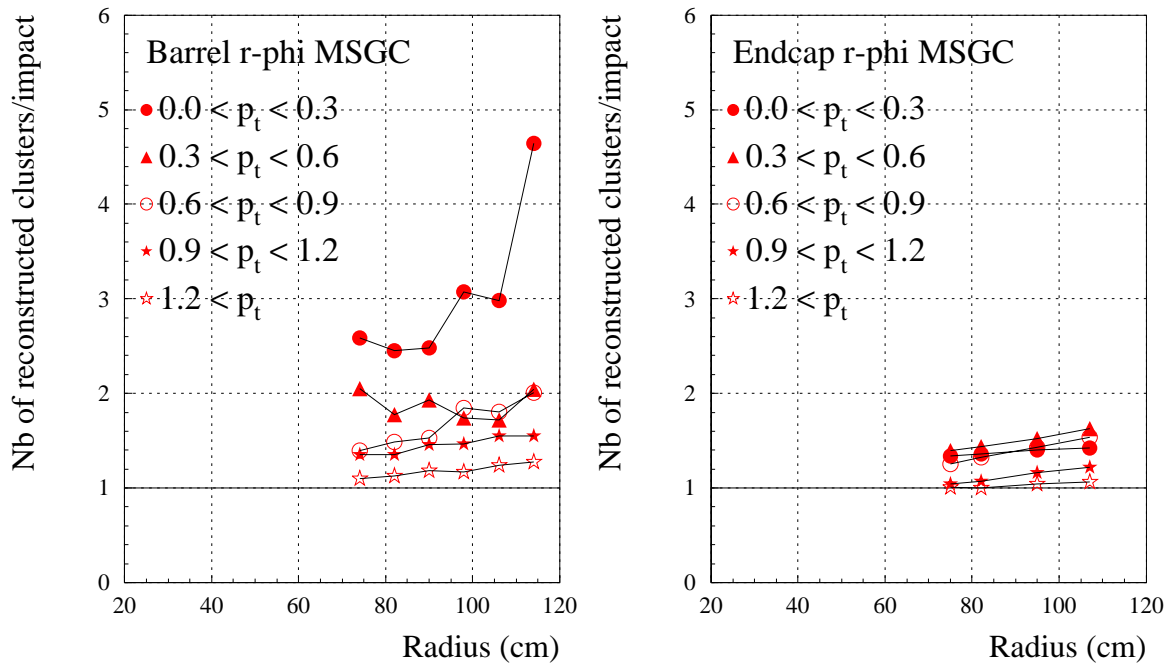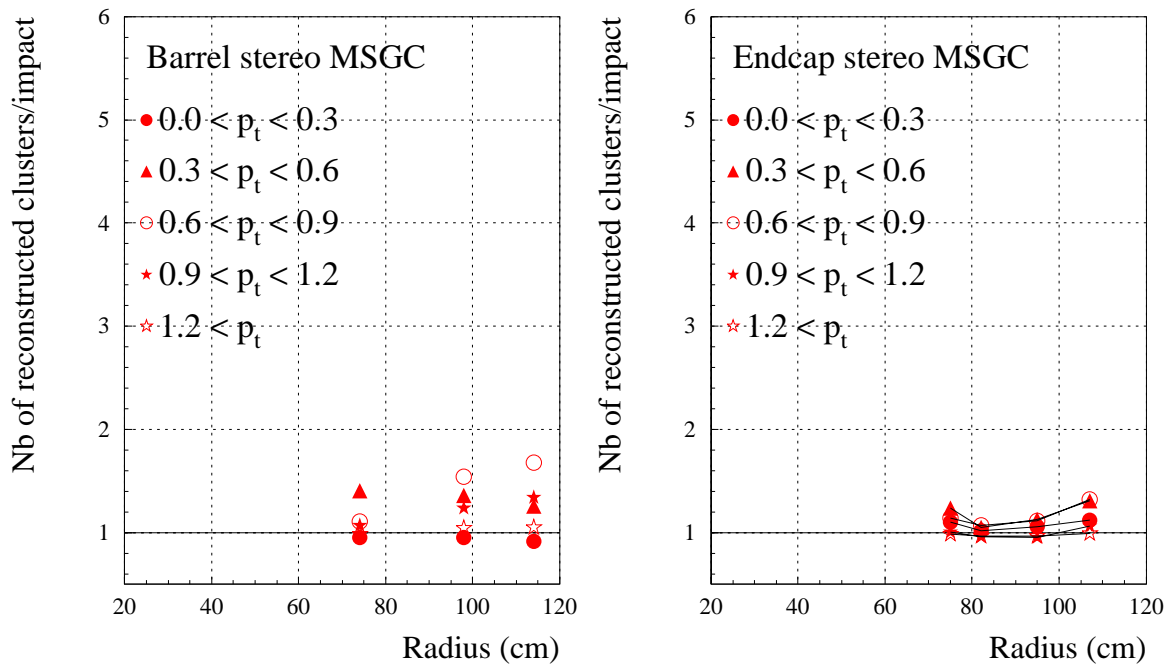


Figure 32: Cluster splitting rate in the stereo barrel (left) and endcap (right) detectors as a function of the detector radius for different ranges of $p_T$ (GeV). (TDR approximation.)

Figure 33: Cluster splitting rate in the r$\phi$ barrel (left) and endcap (right) detectors as a function of the detector radius for different ranges of $p_T$ (GeV). (ORCA detailed simulation)



Figure 34: Cluster splitting rate in the stereo barrel (left) and endcap (right) detectors as a function of the detector radius for different ranges of $p_T$ (GeV). (ORCA detailed simulation)
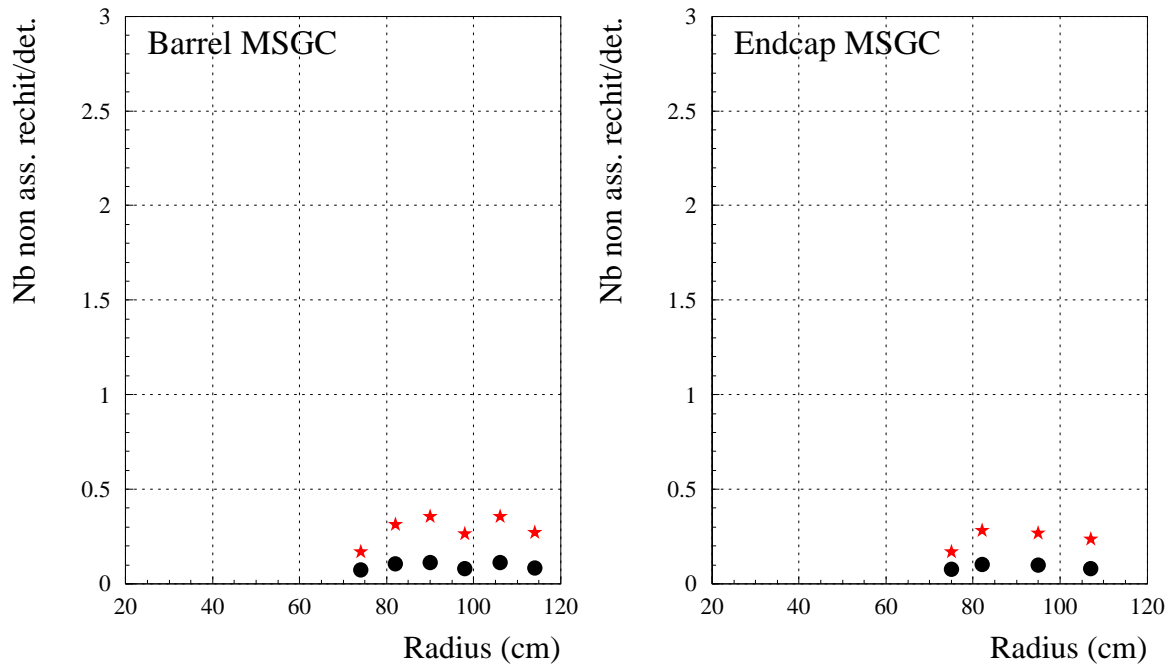
Figure 35: Average number of pure noise clusters per detector, i.e. clusters which are not associated to the charge deposition of a particle. (Circles = TDR approximation; stars = ORCA detailed simulation, with pile-up of 10 bunch-crossings before the trigger event and 2 after.)
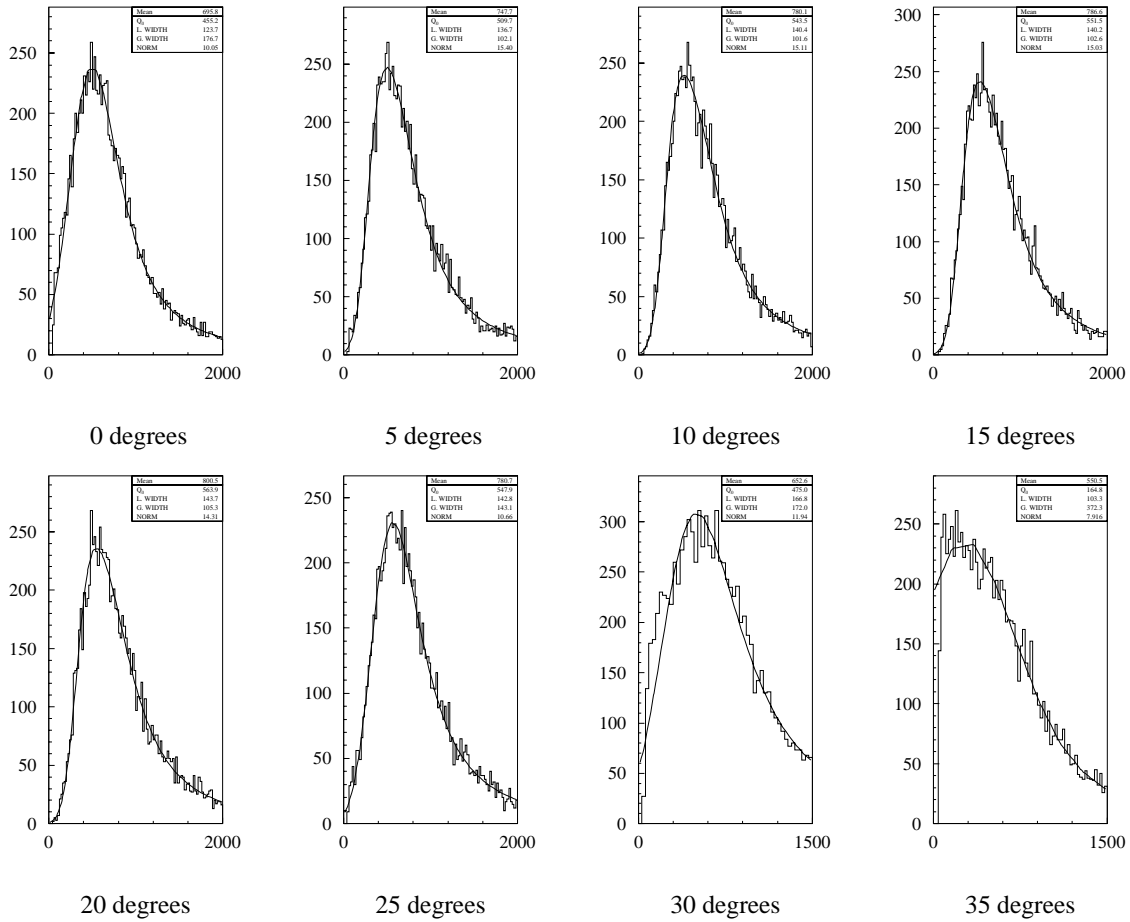
0 degrees      5 degrees      10 degrees      15 degrees

20 degrees      25 degrees      30 degrees      35 degrees

Figure 36: Fits used for the S/N ratio estimates for mip's (0.6 GeV $\pi^-$) as a function of particle incidence angle, in case of no charge loss but for clustering effects, B=4T, with clustering thresholds 1.8-3.5-0.
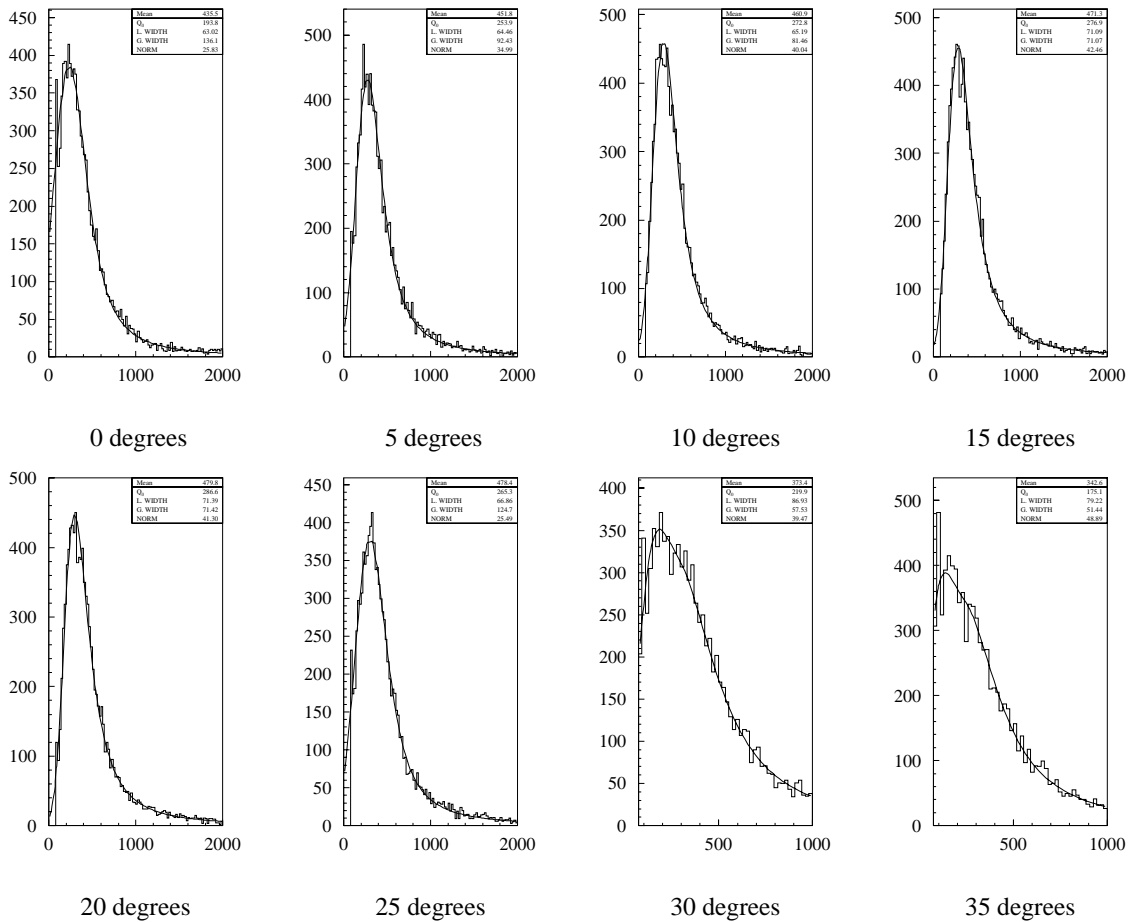
23

Figure 37: Fits used for the S/N ratio estimates for mip's (0.6 GeV $\pi^-$) as a function of particle incidence angle, in deconvolution mode, B=4T, with clustering thresholds 1.8-3.5-0.

24

0 degrees      5 degrees      10 degrees      15 degrees
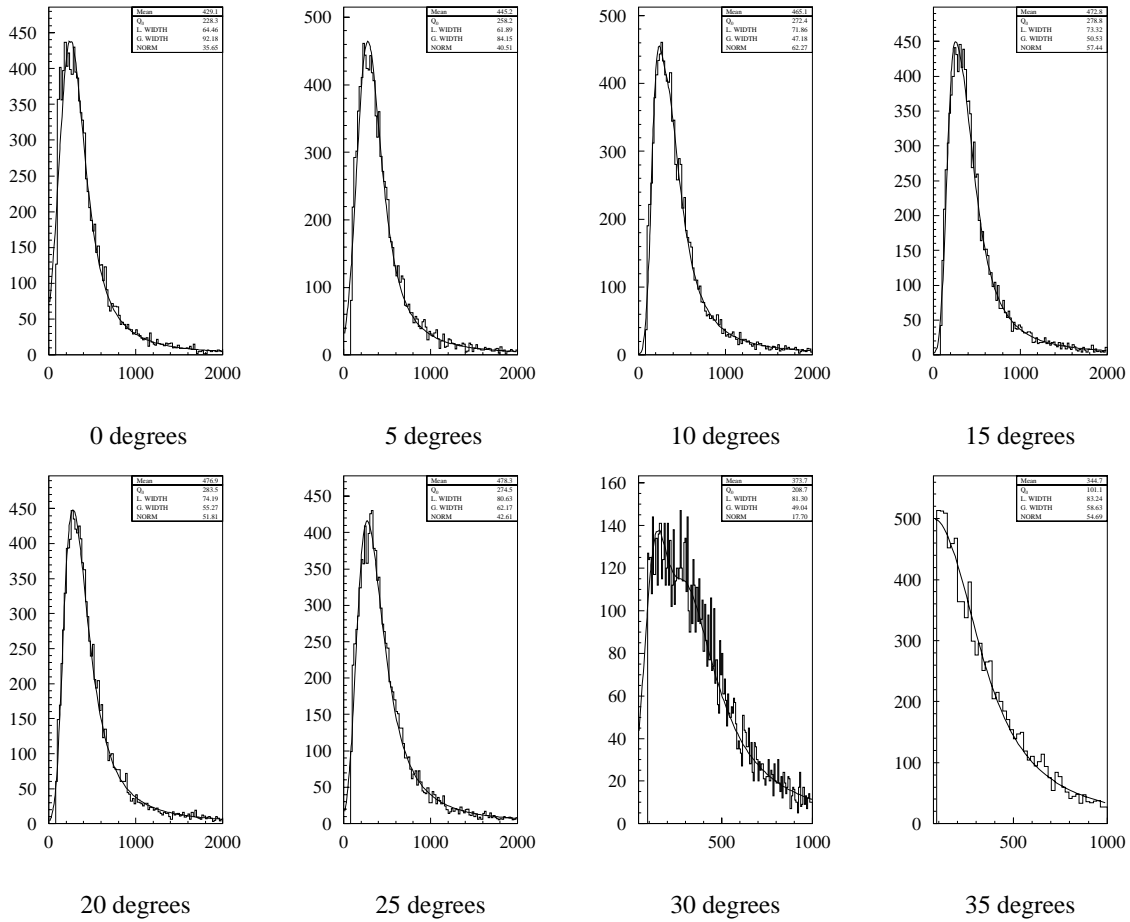
20 degrees      25 degrees      30 degrees      35 degrees

Figure 38: Fits used for the S/N ratio estimates for mip's (0.6 GeV $\pi^-$) as a function of particle incidence angle, in deconvolution mode, B=4T, with clustering thresholds 1.4-0.-4.